EPJ Web of Conferences **67**, 02056 (2014)
DOI: 10.1051/epjconf/20146702056

A new method for fluid input into a hybrid synthetic jet actuator

J. Kordík[1,a], Z. Trávníček[1], and V. Tesař[1]

[1]Institute of Thermomechanics, AS CR

Abstract. A new principle of flow rectification for hybrid synthetic jet actuators is introduced in this paper. As is well known, the flow rectification can be best accomplished by means of fluidic diodes. Novelty of the present study are fluidic diodes with two mutually opposed nozzles. Interaction between the periodic jet flows from the nozzles causes a difference between the blowing and suction strokes, resulting in a particularly efficient rectification effect. The distance between the nozzle exits as well as the oscillation frequency were the parameters, which were varied during hot-wire measurements. The combination of those parameters achieving the highest volumetric efficiency was identified.

1 Introduction

Synthetic jets (SJs), or zero-net-mass-flux jets, are fluid flows generated by the pushing and pulling of the fluid from cavity through an orifice or a nozzle, so that the time mean mass flow through the nozzle is zero. Since the end of the last century, the topic has been intensively investigated [1–3] and many useful applications of synthetic jets have been developed. Hybrid synthetic jets (HSJs, or non-zero-net-mass-flux jets), which were first introduced in [4–6], are very similar to SJs; they are generated by means of non-zero-net-mass flow in the nozzle. The applications of both, SJs and HSJs, may be found especially in boundary-layer separation control [7–9], jet vectoring [10], and heat transfer enhancement [11,12,6,13,14].

There are two basic types of hybrid synthetic jet actuators (HSJAs), which are used for generation of HSJs: The first type combines the usual synthetic jet actuator (SJA) and valveless pump principle. Such HSJA layouts are similar to those of valve-less pumps. They consist of a fluidic diode, an exit nozzle, and a displacement chamber with a moving piston or diaphragm [15–20]. Unlike the valveless pump, the jet flow from the nozzle of the HSJA issues into the ambient space where the HSJ is generated.

The second type of HSJAs uses the fluidic oscillators [21–24]. Their operation requires external flow sources, such as compressors or blowers, and a piping system connecting the source with an actuator nozzle. This type of HSJAs is not investigated in the present paper, which focuses on the first type of HSJA (with an oscillating diaphragm).

The motivation of present paper is based on achieving the same advantages as those offered by HSJA, namely an increase in the velocity of the jet issuing from the nozzle and at the same time decrease the inflow to the nozzle. The outgoing fluid is responsible for formation of the coherent vortical structures in the immediate vicinity of the nozzle exit. The large vortex structures and higher jet velocities increasing the Reynolds number lead to an augmentation of convective heat transfer of the jet [13,6,25] and removal of the already heated (or cooled) fluid from the neighborhood of the heat transfer surface. This is the reason why the HSJAs producing non-zero-net-mass-flux have a great potential in heat transfer applications, even greater than common SJs (this was confirmed experimentally in [13]). The useful applications of HSJs prove that the HSJs are are worthy of an investigation. In addition to that, they represent a new research topic with so far only a few papers focused on their study [4–6,13,21,23,22,14,26–29], therefore experimental investigations of HSJs offer many unexplored possibilities.

To quantify the enhancements of non-zero-net-mass-flux in a nozzle of the HSJA the volumetric efficiency of the HSJA is defined and evaluated. Volumetric efficiency is closely dependent on the performance of the fluidic diode, which is quantified by the diodicity (see [30–33] or diodity [34,35]). It is defined as the ratio of the pressure drops across the diode in the reverse and forward directions. The diodicity is certainly a crucial property, which affects the desirable pumping effect of a HSJA. Today, the vortex diodes are known as the most efficient [36,37,33], but due to their long spin-up and -down time, they are incompatible with the desirable frequency ranges of the current HSJA. The present inlet system of a typical HSJA includes a pair of the fluidic diodes in shape of convergent and divergent channels (similar as are used in [15–19,38]). The diodes are connected to two chambers of HSJAs via their terminals. The outlet cross-sections of these fluidic diodes are arranged as opposite to each other. Outletting and inletting fluid flows between both cross-sections interact so that the diodicity of the input system is enhanced. The aim of this work is to find such combination of actuating frequency and distance between the outlets for a given geometry, which offers the highest possible volumetric efficiency.

[a] e-mail: kordik@it.cas.cz

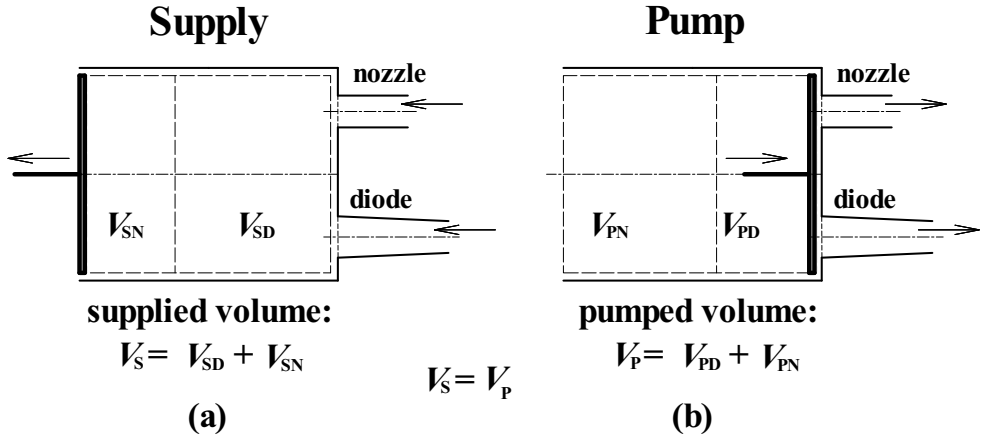

Fig. 1. Principle of the HSJA operating cycle. (a) Supply stroke, (b) Pump stroke.

2 Hybrid synthetic jet principles

As mentioned previously, hybrid synthetic jet actuators are based on the principle of the valveless pump. Figure 1 shows two working strokes, namely the supply and pump (or delivery) stroke, of the valveless pump that is operating with an incompressible fluid. In the first (supply) stroke, the piston (or diaphragm) of the pump moves to the left-hand side, and the fluid is sucked into the actuator cavity. A conical duct element, which was chosen as the fluidic diode here, has a low hydraulic resistance during the inward flow (the forward direction). At the end of the supply cycle, the fluid volume V_{SD} is supplied into the chamber through the diode. The fluid volume sucked into the chamber through the nozzle is denoted as V_{SN}.

In the pump stroke, the fluid is displaced through the fluidic diode, which possesses a higher hydraulic resistance during the outward flow (the reverse direction). This causes the volume V_{PD} of the fluid that passes through the diode during the pump cycle to be less than V_{SD}, and the volume pumped through the nozzle V_{PN} is larger than the volume filled during the supply stroke V_{SN}.

Periodic cycling of the pump and the supply strokes results in a non-zero-net-mass-flux in both the diode and the nozzle. A measure of the pumping efficiency for an incompressible working fluid is the volumetric efficiency, defined by [15] as the following ratio:

$$\varepsilon_V = \frac{V_{PN} - V_{SN}}{V_{SD} + V_{SN}}. \quad (1)$$

Another definition of the volumetric efficiency for hybrid synthetic jets can be introduced as follows:

$$\varepsilon_N = \frac{V_{PN} - V_{SN}}{V_{PN} + V_{SN}}. \quad (2)$$

This is a more user friendly definition because the ε_N is based on the HSJ measurement at the nozzle only without (extremely complicated) measurement of the fluid flux through the diode, namely the term V_{SD} in Eq. (1). This definition (2) was also used as a criterion for comparing the HSJAs in [6,14,26,27] (verbal definition of the volumetric efficiency in [6,14,26] can be easily misunderstood; nevertheless, the application of the formula (2) was confirmed by the authors of the papers). The efficiency ε_N is also used for the investigation of the HSJA in this work.

3 Experimental Setup and Data Processing

3.1 The Design of the Hybrid Synthetic Jet Actuator

The schematic view of the experimental setup and the design of HSJAs is presented in figure 2. The layout of the input system is a subject of the patent application [39]. It has a form of oppositely oriented outlets of conical fluidic diodes. Each diode is connected to its own HSJA. Both actuators are identical and are based on three-inch, high-quality midrange speakers NS3-193-8A (manufactured by AuraSound, Santa Ana, California), which are connected in series. The speakers feature a neodymium ring magnet in a patented underhung geometry that enables a large range of linear excursions of the diaphragm (±4.9 mm).

Each actuator is provided also with one nozzle, from which the HSJ issues.The nozzles of HSJAs, contrary to

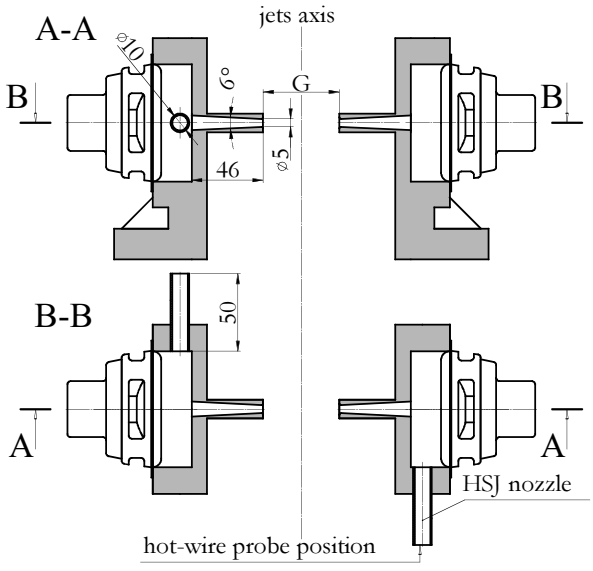

Fig. 2. The design and configuration of HSJAs. A – elevation view, B – ground-plan view

the fludic diodes, are oriented so that the resultant HSJs do not influence each other (aiming at opposite directions, see figure 2). The diameters of the nozzles are 10 mm.

The design of the conical fluidic diodes is taken from [6]: the outlet diameters are 5 mm, the apex angles of the conical duct are 6° and the diode duct lengths are 46 mm. The crucial parameter of the configuration of the HSJAs, which certainly has an effect on the volumetric efficiency, is the diode outlets distance (shown as G in figure 2). To find this effect, the volumetric efficiency was evaluated for 10 values of G between 1 and 20 mm. Apart from the distance G, the driving frequency of the actuator, f, can seriously affect the value of the volumetric efficiency, as well. It was shown in [27], where a HSJA was tested in wide frequency range. Auxiliary experiments were performed with the present configurations of HSJAs and the investigated frequency range was narrowed to: $f = 330 - 370$ Hz. In this range we can expect a maximal value of the volumetric efficiency.

3.2 Data Acquisition and Hardware Setup

The experiments following the evaluation of the volumetric efficiencies ε_N of the HSJA were performed by measuring the velocity profiles at the exit of the actuator nozzle (see figure 2). The MiniCTA 54T30 DANTEC hot-wire anemometer with a single wire probe 55P16 (manufacturer of the anemometer and the probe: Dantec Dynamics A/S, Skovlunde, Denmark) and the NI-PCI 6023E data acquisition device (manufacturer: National Instruments Corporation, Austin, Texas, US) were used. The velocities were measured at a location 0.3 mm outward from the nozzle exit area at 8 points on the nozzle radius. The radial probe coordinates for the measurement in the nozzle were $r = 0.0$, 1.0, 1.9, 2.7, 3.4, 4.0, 4.5 and 5.0 mm. The hot-wire signal was sampled with a sampling frequency of $f \cdot 64$ and the number of samples was 16384. The temperature of the working fluid (air) was measured using a fast-response Pt100 sensor (PT100-SMD0805, time constant is 4 s in air at a speed of 1 m/s; manufacturer: Heraeus Sensor Technology, Kleinostheim, Germany) at the same time as the velocity samples. The measured temperature was used for the temperature correction of the hot-wire data.

The hot-wire probe was calibrated in the velocity range of 0.2 – 53 m/s. The maximum relative uncertainty of a single velocity sample was 14.2%, for very small velocities of 0.2 – 0.4 m/s, and the typical value of the relative uncertainty was below 5% for velocities in range of 0.4 – 53 m/s. A more detailed description of the anemometer settings, probe calibration method, and uncertainty evaluation is available in [40].

During the velocity measurement, the loudspeakers of the actuators were supplied by a harmonic electric current. The effective value of the harmonic electric power $P_{eff} = 1.75$W (total power of both in-series-connected loudspeakers, see Tab. 1) was kept constant and the frequency of the supplied current f was a variable parameter.

Table 1. The parameters of experiments

	Value	Remark
Dimensions:		
$D_2 = 2R_2$	10.0 mm	nozzle diameter
L_2	50.0 mm	nozzle length
$D_3 = 2R_3$	5.0 mm	diode outlet diameter
L_3	46.0 mm	diode duct length
α	6.0°	diode duct apex angle
Fluid properties:		
p_b	97000 Pa	barometric pressure
T_a	293.7 K	air temperature
ρ	1.15 kg/m^3	air density
ν	$1.58 \cdot 10^{-5}$ m^2/s	kinematic viscosity
Actuators input:		
P_{eff}	1.75 W	input effective power
f	330–370 Hz	driving frequency

3.3 Hot-wire Data Reduction

All the measured velocities at particular radial positions were first phase averaged and then, the negative parts of their periods were identified using auxiliary experiments and flipped to negative values; By performing this procedure, the waveforms $U^*(t, r)$ were found. The spatially averaged velocity waveform, which is going to be used in the following evaluations, was found by the integral:

$$U(t) = \frac{1}{\pi R_1^2} \int_0^{R_1} U^*(t, r) \cdot 2\pi r \cdot \mathrm{d}r \tag{3}$$

where R_1 is the nozzle radius.

Auxiliary measurements of the SJs were performed with sealed conical ducts to improve the evaluation of the volumetric efficiencies ε_N of the HSJAs. The velocity waveforms of the SJs were measured at the same input current, locations, and frequencies as the HSJs. The following correction factor g_{SJ} was evaluated from the area-averaged velocities $U(t)$ of the SJ:

$$g_{SJ} = \frac{\int_0^{T_E} U(t)\mathrm{d}t}{\int_{T_E}^{T} |U(t)|\,\mathrm{d}t}, \tag{4}$$

where T_E is the extrusion stroke duration time and T is the period.

The correction factor g_{SJ} was introduced to satisfy the continuity equation and is applied to the negative part of the area-averaged velocity waveform. The factor evaluation method is based on the behavior of the SJ/HSJ, whose velocity streamlines are mostly parallel with the nozzle axis at the nozzle exit during the extrusion stroke (this can be seen, e.g., from the measurements performed in [41] and from the visualization experiments in [14]). Therefore, we can easily estimate the directions of the positive velocities despite the fact that the velocities are measured by a single wire probe, which cannot distinguish the flow direction. This is the reason that the integration of the measured velocity $U(t)$ from 0 to T_E gives a precise result for the extruded fluid volume.

Conversely, the fluid is sucked from a large area near the nozzle outlet during the suction stroke, and streamlines are not parallel to the axis, but they are centripetal in character. Therefore, the negative part of $U(t)$, which relates

to the suction stroke, will be corrected with respect to the continuity equation.

The volumetric efficiency of the HSJ is evaluated by means of Eqs. (2) and (4):

$$\varepsilon_{\mathrm{N}} = \frac{\int_0^{T_{\mathrm{E}}} U(t)\mathrm{d}t - g_{\mathrm{SJ}} \int_{T_{\mathrm{E}}}^{T} |U(t)|\,\mathrm{d}t}{\int_0^{T_{\mathrm{E}}} U(t)\mathrm{d}t + g_{\mathrm{SJ}} \int_{T_{\mathrm{E}}}^{T} |U(t)|\,\mathrm{d}t}, \qquad (5)$$

where the factor g_{SJ} is obtained from the auxiliary SJ measurements.

4 Experimental Results

The resultant volumetric efficiencies as functions of the driving frequency are plotted in figure 3. Peaks of the graphs for different values of G are not sharp. They can be located in the interval of $f = 360 - 370$ for G > 2 mm.

The next figure 4 presents the other view: the volumetric efficiencies are found here for functions of the distance G. The more prominent peaks can be found for the driving frequencies $f > 345$. The optimum value for the distance G seems to be around 10 mm.

Figure 5 displays the results from Figs. 3 and 4 in a 3D space – in form of volumetric efficiency contours. The conclusion that follows from figure 5 is the maximum of volumetric efficiency $\varepsilon_{\mathrm{N}} \approx 0.17$ may be expected in the rectangle: $f = 360 - 370$ Hz $\times$ $G = 7 - 12$ mm.

5 Conclusion

Volumetric efficiency of a HSJA with a new fluid input system was examined experimentally in this paper. The input was designed as two conical fluidic diodes, whose outlets were oriented oppositely to each other. The distance of the outlets and the HSJA driving frequency were the varied parameters during the experiments. The highest volumetric efficiency, about 0.17, was found for combination of the outlets distance 7–12 mm and driving frequencies 360–370 Hz.

Acknowledgement

We gratefully acknowledge the support of the Grant Agency CR (project numbers P101/12/P556 and P101/11/J019) and the institutional support RVO:61388998.

References

1. B.L. Smith, A. Glezer, Phys. Fluids **10**, 2281 (1998)
2. A. Glezer, M. Amitay, Annu. Rev. Fluid Mech. **34**, 503 (2002)
3. J.E. Cater, J. Soria, J. Fluid Mech. **472**, 167 (2002)
4. Z. Trávníček, A. Fedorchenko, A.B. Wang, *An enhancement of synthetic jets by means of an integrated valveless pump*, in *Proceedings of the Tenth Asian Congress of Fluid Mechanics (ACFMX)*, edited by J.J. Wijetunge (Peradeniya, 2004), pp. 535–540

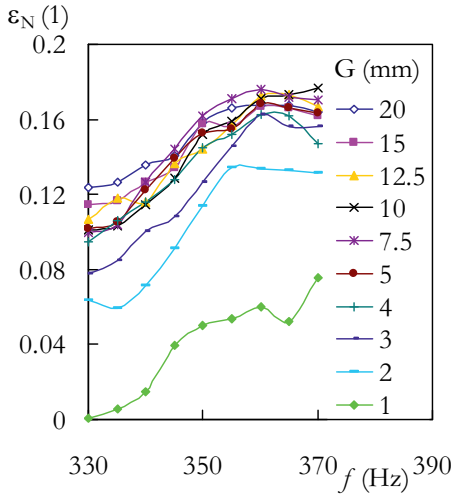

Fig. 3. Volumetric efficiencies as functions of the distance G.

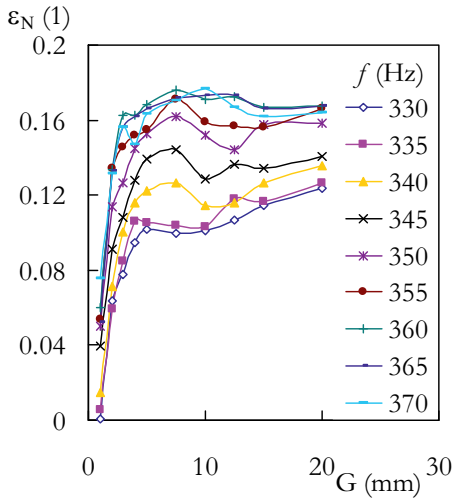

Fig. 4. Volumetric efficiencies as functions of the actuating frequency.

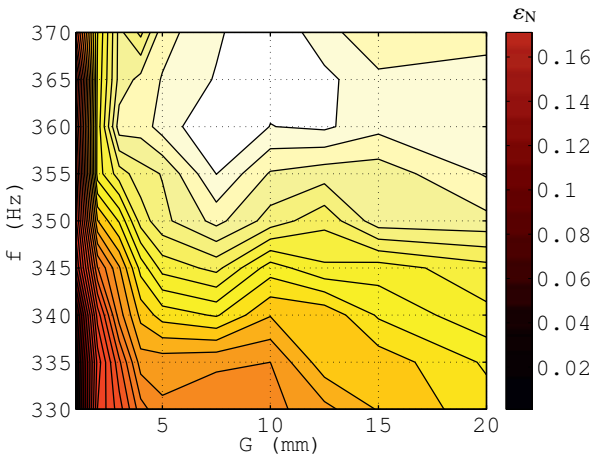

Fig. 5. Contours of the measured volumetric efficiencies.

5. Z. Trávníček, A. Fedorchenko, A.B. Wang, Sensor Actuat. A-Phys. **120**, 232 (2005)
6. Z. Trávníček, T. Vít, V. Tesař, Phys. Fluids **18**, 081701 (2006)
7. G. Hong, Sensor Actuat. A-Phys. **132**, 607 (2006)
8. J. Dandois, E. Garnier, P. Sagaut, J. Fluid Mech. **574**, 25 (2007)
9. D. You, P. Moin, J. Fluid Struct. **24**, 1349 (2008)
10. B.L. Smith, A. Glezer, J. Fluid Mech. **458**, 1 (2002)
11. M.B. Gillespie, M.S. thesis, Georgia Institute of Technology (1998)
12. Z. Trávníček, V. Tesař, Int. J. Heat Mass Transfer **46**, 3291 (2003)
13. Z. Trávníček, T. Vít, *Hybrid synthetic jet intended for enhanced jet impingement heat/mass transfer*, in *13th International Heat Transfer Conference IHTC-13* (Sydney, 2006), p. 12
14. Z. Trávníček, V. Tesař, J. Kordík, J. Visual. **11**, 221 (2008)
15. E. Stemme, G. Stemme, Sensor Actuat. A-Phys. **39**, 159 (1993)
16. T. Gerlach, H. Wurmus, Sensor Actuat. A-Phys. **50**, 135 (1995)
17. A. Olsson, G. Stemme, E. Stemme, Sensor Actuat. A-Phys. **57**, 137 (1996)
18. T. Gerlach, Sensor Actuat. A-Phys. **69**, 181 (1998)
19. A. Olsson, O. Larsson, J. Holn, L. Lundbladh, O. Ohman, G. Stemme, Sensor Actuat. A-Phys. **64**, 63 (1998)
20. C.J. Morris, F.K. Forster, J. Micromech. Microeng. **10**, 459 (2000)
21. V. Tesař, C. Hung, W. Zimmerman, Sensor Actuat. A-Phys. **125**, 159 (2006)
22. V. Tesař, Sensor Actuat. A-Phys. **138**, 394 (2007)
23. V. Tesař, Z. Trávníček, J. Kordík, Z. Randa, Sensor Actuat. A-Phys. **138**, 213 (2007)
24. G. Arwatz, I. Fono, A. Seifert, AIAA J. **46**, 1107 (2008)
25. T. Persoons, A. McGuinn, D.B. Murray, Int. J. Heat Mass Transfer **54**, 3900 (2011)
26. S.S. Hsu, J. Kordík, Z. Trávníček, A.B. Wang, J. Flow Visual. Image Proc. **19**, 1 (2012)
27. J. Kordík, Z. Trávníček, Journal of Fluids Engineering **135**, 101101 (2013)
28. V. Tesař, J. Kordík, Sensors and Actuators A: Physical **199**, 391 (2013)
29. V. Tesař, J. Kordík, Sensors and Actuators A: Physical **199**, 379 (2013)
30. R.L. Bradel, PhD Thesis, University of Washington, Washington (2000)
31. F.K. Forster, B.E. Williams, *Parametric design of fixed-geometry microvalves – the Tesser valve*, in *ASME International Mechanical Engineering Congress & Exposition, IMECE2002* (IMECE2002-33628, New Orleans, 2002), p. 7
32. A.R. Gamboa, C.J. Morris, F.K. Forster, J. Fluids Eng-Trans ASME **127**, 339 (2005)
33. A.A. Kulkarni, V.V. Ranade, R. Rajeev, S.B. Koganti, Chem. Eng. Sci. **64**, 1285 (2009)
34. V. Tesař, *Pressure-Driven Microfluidics* (Artech House Publishers, Norwood, 2007)
35. V. Tesař, in *Encyclopedia of Microfluidics and Nanofluidics*, edited by D. Li (Springer Science + Business Media, New York, 2008), pp. 2131–2139
36. G.H. Priestman, J.R. Tippetts, *Factors affecting the application of vortex diodes and throttles*, in *Proceedings of the Symposium Fluid Control and Measurement (FLUCOME)*, edited by M. Harada (Pergamon, Oxford, 1985), pp. 241–246
37. F. Haakh, J. of Hydraulic Res. **41**, 53 (2003)
38. Z. Liu, Y. Deng, S. Lin, M. Xuan, Engineering Optimization **44**, 1389 (2012)
39. Z. Trávníček, V. Tesař, J. Kordík, A.B. Wang, S.S. Hsu, Patent PV 2012-423 (2012)
40. J. Kordík, PhD Thesis, Czech Technical University, Prague (2011)
41. G.M. Di Cicca, G. Iuso, Fluid Dyn. Res. **39**, 673 (2007)